Journal of Solid State Chemistry 288 (2020) 121434

Contents lists available at ScienceDirect

Journal of Solid State Chemistry

journal homepage: www.elsevier.com/locate/jssc

The role of Fe^{3+} ions in fluorescence detection of H_2S by a bimetallic metal-organic framework

Zan Zhu, Varun Natarajan, Wei-Ning Wang **

Department of Mechanical and Nuclear Engineering, Virginia Commonwealth University, Richmond, VA, 23219, USA

ARTICLE INFO

Keywords:
Turn-off
Fluorophore identification
Disease diagnosis
MOF decomposition

ABSTRACT

A novel bimetallic MOF (i.e., Fe_xAl_{1-x}-MIL) with fluorescence quenching in the probe, was constructed to detect H_2S based on a "turn-on" effect in an aqueous system. Interestingly, a trace amount of Al^{3+} replaced by Fe^{3+} in the parent MOF Al-MIL-53-NH_2 causes significant fluorescence quenching in the bimetallic MOF, which is attributed to the strong ligand to metal charge transfer between unpaired electrons in Fe^{3+} and π-conjugated BDC-NH_2 ligands. After H_2S treatment, a fluorescence augmentation was observed, with a good linear relationship between H_2S concentration (0–38.46 μM) and fluorescence intensity, indicating that $Fe_{0.05}Al_{0.95}$-MIL could be used for quantitative H_2S detection. Particularly, Fe^{3+} in the bimetallic MOF seized by S^{2-} facilitated the partial degradation and subsequent release of BDC-NH_2 ligands, which were determined to be real fluorophores that contributed to the fluorescence enhancement. This study offers new insights into the luminescent bimetallic MOF design and would expand its application in chemical sensing.

1. Introduction

Hydrogen sulfide (H_2S) is one of the most important signaling molecules as it is closely related to physiological and pathological processes in biological systems [1–4]. Over the past decades, many research efforts have been dedicated to the development of chemical sensors towards H_2S at a cellular level because of their potential applications in diagnosing many complex diseases such as acute pancreatitis [3], Parkinson's disease [5], diabetes [6], Alzheimer's disease [7], and periodontal disease [8].

Fluorescence-based sensing technique is a promising analytical method for H_2S detection due to its high sensitivity, desirable selectivity, short response time, and readily visible imaging [9–14]. In particular, a fluorescence-based "turn-on" strategy is preferred to avoid false responses and unexpected signal-to-noise ratios (S/N), considering the detection usually occurs in a dark background [15]. The typical reactions based on the fluorescence "turn-on" effect can be categorized as follows: (1) nitro/azide reduction [16]; (2) coordination of H_2S with auxochromic groups [17]; and (3) transitional metals (e.g., Cu^{2+} and Ag^{+}) replacement [18].

Up to the present time, various luminescent probes have been developed for H_2S detection. Among these probes, metal-organic frameworks (MOFs), a class of porous crystalline polymers built from metal ions/clusters and organic ligands, have gained considerable attention because of their versatile and tunable optical properties [19–23]. To realize the "turn-on" effect, ligand functionalization of luminescent MOFs is a widely used approach. The brief description of the "turn-on" process is as follows. First, before H_2S detection, the MOFs should be in the "turn-off" mode, which can be achieved by adding organic ligands containing azide or nitro groups. These strong electron-withdrawing groups can trap the most absorbed exciting energy and cause a quickly running internal singlet-triplet conversion, thus limiting the fluorescence emission [24–26]. Once treated by H_2S, these azide and nitro groups will be reduced to electron-donating amine groups, leading to less internal energy dissipation, and therefore, a fluorescence enhancement is observed. Another interesting approach is to introduce specific transitional metal ions (e.g., Cu^{2+} and Ag^{+}) that have high affinity with S^{2-} to the lanthanide-based (e.g., Eu and Tb) MOFs through a "one-pot" wet chemistry route or post-modification [15,27,28]. Likewise, the fluorescence "turn-on" effect would also show up after silver/copper sulfide precipitation. However, most reported probes based on the above methods showed undesirable performance towards H_2S detection at a lower concentration (0–100 μM), which is mainly caused by the incomplete quenching in materials before H_2S treatment and insignificant resulting fluorophores released after being exposed to H_2S.

* Corresponding author.
E-mail address: wnwang@vcu.edu (W.-N. Wang).

https://doi.org/10.1016/j.jssc.2020.121434
Received 12 April 2020; Received in revised form 2 May 2020; Accepted 4 May 2020
Available online 11 May 2020
0022-4596/© 2020 Elsevier Inc. All rights reserved.

Recently, bimetallic MOFs have emerged as an option to create multiple functionalities by mixing two different metal ions as nodes in their framework [29,30]. Since the fluorescent properties of MOFs are determined by the energy transfer between metal ions and ligands, the secondary incorporated metal ions in the parent MOF would provide more versatilities during the sensing process, making bimetallic MOFs a great platform for chemical detection. Some lanthanide-based MOFs discussed above were reported to contain different transitional metal ions (e.g., Cu^{2+} and Ag^{+}) in the material [15,27,28], which makes them appear like "bimetallic MOFs". Nevertheless, these doped metal ions were simply bonded to ligands without replacing the original metal nodes in the framework, which makes the quenching effects in parent MOFs less effective. Therefore, complicated post-modification and a relatively large amount of quenching materials are often needed to keep MOFs from emitting fluorescence. Furthermore, the high expense of lanthanide elements or rare-earth elements also restricts their further development and practical application. Given bimetallic MOFs containing the secondary substitutional metal ions as constructing nodes were rarely reported for H_2S detection, an efficient fluorescence quencher in parent MOF but with the ability to induce the "turn-on" effect is in urgent demand.

Herein, we report a novel bimetallic MOF, i.e., Fe_xAl_{1-x}-MIL for H_2S detection in an aqueous system. Within this bimetallic MOF, two cost-effective and earth-abundant transitional metals (Fe^{3+} and Al^{3+}) were used as constructing nodes, while 2-aminobenzene-1,4-dicarboxylic acid (BDC-NH_2) was applied as a bridging ligand. In addition to Fe^{3+}, other trivalent metal ions, such as Cr^{3+}, V^{3+}, and Ru^{3+} also have similar quenching effects since they have similar electron configurations with Fe^{3+} where *d* orbitals are not fully filled. The partially filled *d* orbitals act as energy acceptors to receive the feedback electrons from the linkers, leading to a fluorescence quenching in the system [34,35]. However, these metal ions are generally expensive and not environmentally friendly, hence they were not studied in the present study.

In this study, the parent MOF, Al-MIL-53-NH_2, is the support matrix as it produces strong blue fluorescence with the existence of $–NH_2$ group [31]. Fe^{3+} is a strong fluorescence quencher used in many luminescent MOF probes due to its partially filled *d* orbitals that can be served as the energy acceptor in the system [32,33]. Because of the partial Fe substation with Al ions in the Al-MIL-53-NH_2 framework, a strong ligand to metal charge transfer (LMCT) was generated between Fe^{3+} ions and BDC-NH_2 ligands, which made the quenching effect extremely efficient within the bimetallic MOF. When $Fe_{0.05}Al_{0.95}$-MIL was exposed to H_2S (0–38.46 μM), a "turn-on" effect was observed and a good linear relationship was also obtained between fluorescence intensity and H_2S concentration, indicating the bimetallic MOF could be used for selective and quantitative H_2S detection. To unravel the mechanism of fluorescence enhancement, systematic characterizations and analyses were conducted on both remained undissolved particles and supernatants. The results showed that during the H_2S sensing process, Fe^{3+} in the bimetallic MOF was "pulled out" and seized by S^{2-} to form Fe_2S_3, which was subsequently converted to FeS and S. Then the FeS would be further oxidized to Fe^{3+} and SO_4^{2-} in the presence of air. Additionally, the $Fe_{0.05}Al_{0.95}$-MIL was proved to be partially decomposed after H_2S treatment, and the released BDC-NH_2 ligands were determined to be real fluorophores that contributed to the fluorescence enhancement. We believe that the outcome of this work could shed light on the rational design of fluorescence-based bimetallic MOFs for chemical sensing.

2. Experimental section

2.1. Chemicals

Aluminum chloride hexahydrate ($AlCl_3·6H_2O$, 99%), Ion chloride hexahydrate ($FeCl_3·6H_2O$, 99%), and 2-amino-1,4-dicarboxylic acid ($C_8H_7NO_4$, BDC-NH_2, 99%) were purchased from Sigma-Aldrich. Acetone (C_3H_6O, 99.5%), N, N-dimethylformamide ($HCON(CH_3)_2$, DMF) were obtained from VWR Corporation. Ethanol (C_2H_5OH, 190 proof) was purchased from Gold Shield. Deionized (DI) water was used to prepare solutions. All chemicals were used without further purification.

2.2. Material synthesis

Al-MIL-53-NH_2. Al-MIL-53-NH_2 was synthesized based on a previous report [36]. A mixture of $AlCl_3·6H_2O$ (1.45 g), NH_2-BDC (1.1 g) and 50 ml DI water was heated using a 100 ml Teflon lined steel autoclave at 150 °C for 5 h. The obtained precipitates were washed with DMF three times and subsequently activated. The activation was conducted by immersing as-synthesized crude materials in 60 ml DMF at 155 °C for 12 h. The above activation procedure was repeated a second time. Finally, the pale-yellow particles were dried at 155 °C in the air for 24 h.

Fe_xAl_{1-x}-MIL (x = 0.05, 0.1, and 0.2). In a typical procedure, mixtures of $AlCl_3·6H_2O$, $FeCl_3·6H_2O$, and NH_2-BDC with different ratios were suspended in 50 ml DI water and then heated using a 100 ml Teflon lined steel autoclave at 150 °C for 5 h. Detailed precursor compositions are listed in Table 1. The obtained particles were washed with DMF three times and subsequently activated. The as-synthesized materials were kept in 60 ml DMF at 155 °C for 12 h. The above activation procedure was repeated a second time. Finally, the orange particles were dried at 155 °C in the air for 24 h. In this study, the activated bimetallic MOFs are labeled as Fe_xAl_{1-x}-MIL with the Fe/Al molar ratios indicated by the precursors' molar ratio in the subscript. It should be noted that this value does not represent the actual Fe/Al molar ratio in the final product. The precise experimental Fe/Al ratios were determined by EDX (energy-dispersive X-ray spectroscopy), which are discussed in the next section.

Fe-MIL-53-NH_2. Fe-MIL-53-NH_2 was synthesized according to a previous study [37]. A mixture of $FeCl_3·6H_2O$ (1.35 g), NH_2-BDC (0.9 g) and 50 ml DI water was placed in the 100 ml Teflon-sealed steel autoclave and heated in an oven at 150 °C for 48 h. The precipitates were washed with DI water, DMF, and acetone, respectively. Then the as-synthesized crude materials were activated in 15 ml ethanol at 150 °C for 48 h. The above activation procedure was repeated a second time. The resulting dark brown solids were recovered by centrifuge and dried in air at 150 °C.

2.3. Materials characterization

The structure of as-synthesized materials was analyzed by powder X-ray diffraction (PXRD) using a PANalytical X'Pert Pro MPD diffractometer. Element mapping was conducted using an SEM (scanning electron microscope, Su-70, Hitachi) equipped with energy-dispersive X-ray spectroscopy (EDX). Vibration analysis of functional groups was carried out with a Fourier transform infrared (FT-IR) spectrometer (Nicolet iS50, Thermo Scientific). The optical absorption spectra were obtained from the UV–Vis measurements using an Evolution UV-220 spectrophotometer. Fluorescence properties of the samples were characterized by a fluorescence spectrometer (PTI QuantaMaster-400). The quantum yields (QY) were determined as the integrated intensity of the luminescence signal divided by that of absorption. The absorption integrated intensity was measured by subtracting the luminescence signal from the blank reference sample in an integrating sphere. X-ray photoelectron

Table 1
Precursor compositions for Fe_xAl_{1-x}-MIL

Samples	DI (ml)	$FeCl_3·6H_2O$ (g)	$AlCl_3·6H_2O$ (g)	Fe:Al Mole Ratio	BDC-NH_2 (g)
$Fe_{0.05}Al_{0.95}$-MIL	50	0.081	1.37	0.05:0.95	1.1
$Fe_{0.1}Al_{0.9}$-MIL	50	0.162	1.30	0.1:0.9	1.1
$Fe_{0.2}Al_{0.8}$-MIL	50	0.324	1.16	0.2:0.8	1.1

spectroscopy (XPS, Thermo Scientific ESCALAB 250) was used to investigate the chemical state of the elements on the surface of the samples.

2.4. H_2S fluorescence sensing measurements

NaHS was used as the H_2S source and dissolved in DI water to form a transparent solution [1]. In this study, "H_2S treated" or "H_2S treatment" means that the samples are suspended in NaHS solution with a specific concentration. In a typical experiment, 0.7 mg bimetallic MOF was suspended in a cuvette containing 3 ml DI water. A varying volume (0–140 μL) of NaHS (1.0 mM) solution was then added into the above MOF suspension and the spectrum was taken within 90 s. The corresponding supernatant and suspended undissolved particles were separated by centrifugation at 12000 rpm for 5 min. Another fluorescence measurement of the re-collected particles that were resuspended into 3.0 ml DI water was conducted for comparison. For the fluorescence measurements, the excitation wavelength was fixed at 330 nm and the emission spectra were recorded in the range from 380 nm to 580 nm. Both the emission and excitation slits were set to be 2 nm.

3. Results and discussion

3.1. Materials characterization

A "one-pot" hydrothermal method was utilized for the synthesis of bimetallic MOFs, where the substitution of Fe atoms in the Al-MIL-53-NH_2 framework was achieved by adjusting the mole ratio of Fe to Al from 0.05 to 0.2 in the precursor. As shown in Fig. 1a-e, with increasing Fe/Al ratios, the color of Fe_xAl_{1-x}-MIL gradually turned from yellow to the dark brown, indicating the successful substitution of Fe^{3+} with partial Al^{3+} inside the framework. The element composition within $Fe_{0.05}Al_{0.95}$-MIL was also confirmed by EDX analysis. The results showed that altering the Fe/Al ratio from 0.05 to 0.2 led to the Fe/Al ratio in products changing from 0.048 to 0.181 (Table S1), which indicates that the percentage of Fe in Fe_xAl_{1-x}-MIL can be tuned by simply changing the starting Fe concentration in the precursor. Moreover, elemental mapping of $Fe_{0.05}Al_{0.95}$-MIL (Fig. 1f-i) confirms the uniform distribution of Fe within the Al-MIL-53-NH_2 matrix.

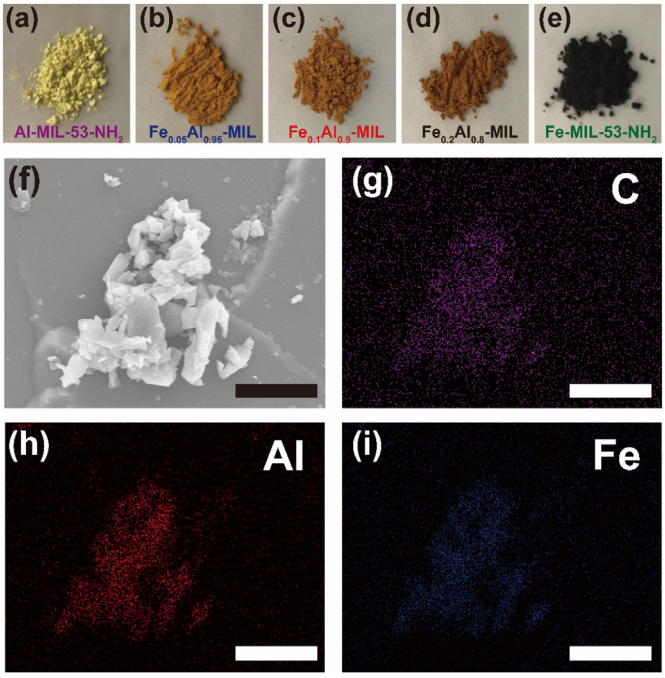

Fig. 1. Digital images of Al-MIL-53-NH_2 (a), Fe_xAl_{1-x}-MIL (x = 0.05, 0.1, and 0.2) (b–d), and Fe-MIL-53-NH_2 (e); SEM image (f) and elemental mapping (g–i) of $Fe_{0.05}Al_{0.95}$-MIL (f). Scale bars: 10 μm.

In addition to the investigations on the morphology and chemical composition, structure analysis was conducted by PXRD. As shown in Fig. 2a, all the Fe_xAl_{1-x}-MIL (x = 0.05, 0.1, and 0.2) and Al-MIL-53-NH_2 exhibited the same PXRD patterns, indicating these as-synthesized bimetallic MOFs maintained a structure similar to that of Al-MIL-53-NH_2. Specifically, the framework of Fe_xAl_{1-x}-MIL is built from AlO_6 octahedra connected via trans-bridging OH ions and carboxylate moieties from BDC-NH_2 linkers but with different amounts of Fe substitution of Al in pure parent Al-MIL-53-NH_2, as shown in Fig. 2b [38,39]. It should be noted that no phases of Fe-MIL-53-NH_2 were observed in the PXRD patterns of Fe_xAl_{1-x}-MIL, which demonstrated that the as-prepared bimetallic MOFs are indeed MOFs with different metallic nodes rather than a mixture of monometallic MOFs [40]. Furthermore, we conducted a high-resolution PXRD scan for peak (110) from 12.0° to 12.8° (Fig. 2c). Interestingly, the position of peak (110) shifts from 12.46° to a lower angle of 12.29° with increased Fe concentration in the products (Fig. 2d). This can be explained based on the well-known Bragg's law:

$$d = \frac{n\lambda}{2\sin\theta}$$

where d is the interplanar spacing of (110); n is the positive integer (1); λ is the X-ray wavelength (λ= 1.5406 Å); θ is the Bragg angle. A smaller Bragg angle of Fe_xAl_{1-x}-MIL corresponds to a larger (110) interplanar spacing (Fig. 2d), namely, the lattice of framework expands with more Fe substitution of Al in the Al-MIL-53-NH_2 matrix. This phenomenon is likely caused by the replacement of the larger atomic radii of Fe (156 pm) with Al (118 pm) [41].

Further evidence of Fe substitution within the Al-MIL-53-NH_2 matrix was studied using an XPS. Herein, we select $Fe_{0.05}Al_{0.95}$-MIL as a representative bimetallic MOF. To analyze the effects on the coordination environment caused by Fe substitution, high-resolution XPS spectra of Fe 2p and O 1s were obtained, as shown in Fig. 3. Clearly, no Fe signal was captured in Al-MIL-53-NH_2 while apparent Fe^{3+} peaks (Fe $2p_{3/2}$ at 724.9 eV and Fe $2p_{1/2}$ at 711.3 eV) were observed in $Fe_{0.05}Al_{0.95}$-MIL, demonstrating successful substitution of Fe in Al-MIL-53-NH_2. [40] Fig. 3b shows the high-resolution XPS spectra of O 1s for both Al-MIL-53-NH_2 and $Fe_{0.05}Al_{0.95}$-MIL. The peaks at 531.4 eV, 532.2 eV, and 532.7 eV for both samples are attributed to the Al–O, O–C═O, and C–O bonds, respectively [42,43]. In particular, the peak at 530.1 eV in the orange shadow was observed in $Fe_{0.05}Al_{0.95}$-MIL (Fig. 3b), which was ascribed to the existence of a newly constructed Fe–O bond [44]. Such well-founded evidence of Fe in the O 1s spectrum of $Fe_{0.05}Al_{0.95}$-MIL once again suggests that Fe ions have been successfully incorporated into the framework, which is well consistent with the results shown in Fig. 1.

3.2. Optical properties and H_2S sensing

To elucidate the behavior of Fe ions within the bimetallic MOF, the optical responses of BDC-NH_2, Al-MIL-53-NH_2, $Fe_{0.05}Al_{0.95}$-MIL, and Fe-MIL-53-NH_2 were examined by UV–vis spectroscopy. As displayed in Fig. 4a, the MOFs (e.g., Al-MIL-53-NH_2, $Fe_{0.05}Al_{0.95}$-MIL, and Fe-MIL-53-NH_2) share similar absorption spectra with the bridging linker BDC-NH_2 within the UV region, where one intense peak at 280 nm is ascribed to the $\pi \rightarrow \pi^*$ electronic transitions of the aromatic ring and the other peak in the range of 300–420 nm is originated from the introducing NH_2 groups from BDC-NH_2 [45,46]. For Fe-MIL-53-NH_2, the wide band over the entire visible region is due to the spin-allowed *d-d* transition of Fe^{3+} ($^6A_{1g} \rightarrow {}^6A_{1g} + {}^4E_g(G)$) [47,48], which is also observed in bimetallic MOF $Fe_{0.05}Al_{0.95}$-MIL. In general, the Al-MIL-53-NH_2 has no absorption in the visible region, while Fe-MIL-53-NH_2 shows strong visible light absorption. The UV–vis spectra of $Fe_{0.05}Al_{0.95}$-MIL showed features of both components, and the absorption in the visible region becomes stronger with increasing Fe contents in the bimetallic MOF (Fig. S1), which further supports the successful incorporation of Fe in the bimetallic MOF.

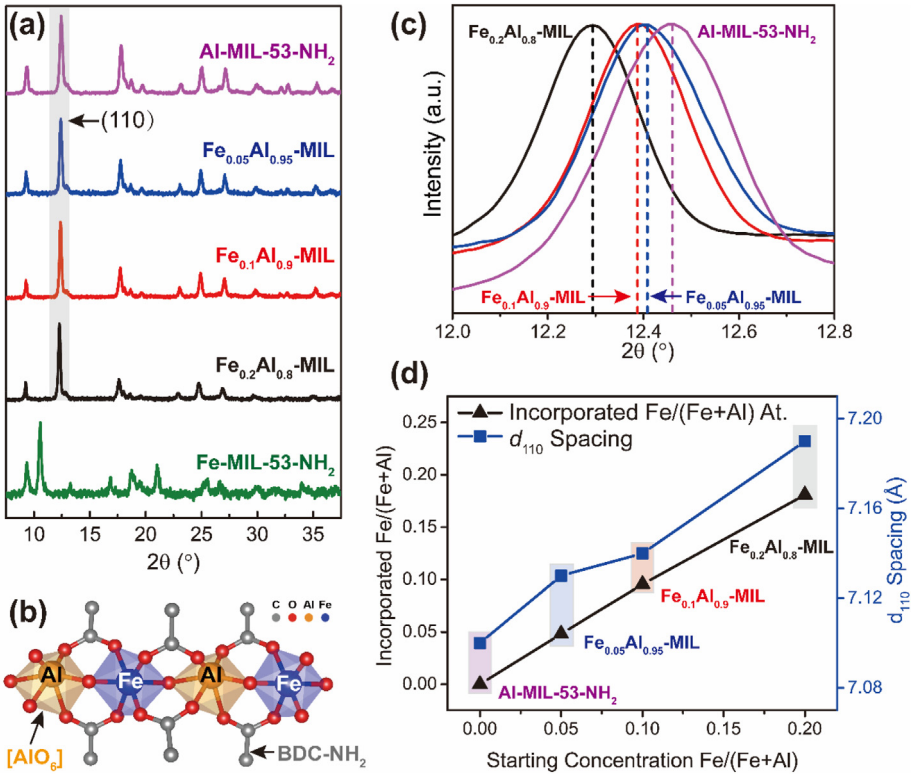

Fig. 2. (a) PXRD patterns of Al-MIL-53-NH_2, Fe_xAl_{1-x}-MIL, and Fe-MIL-53-NH_2; (b) Fe_xAl_{1-x}-MIL with a ball and stick representation of a site-isolated Fe within the MIL-53-NH_2 octahedra [AlO_6] chain; (c) High-resolution PXRD scan at (110) peak of Al-MIL-53-NH_2 and Fe_xAl_{1-x}-MIL; (d) d_{110} spacings and incorporated Fe concentrations in products versus Fe concentration in precursors.

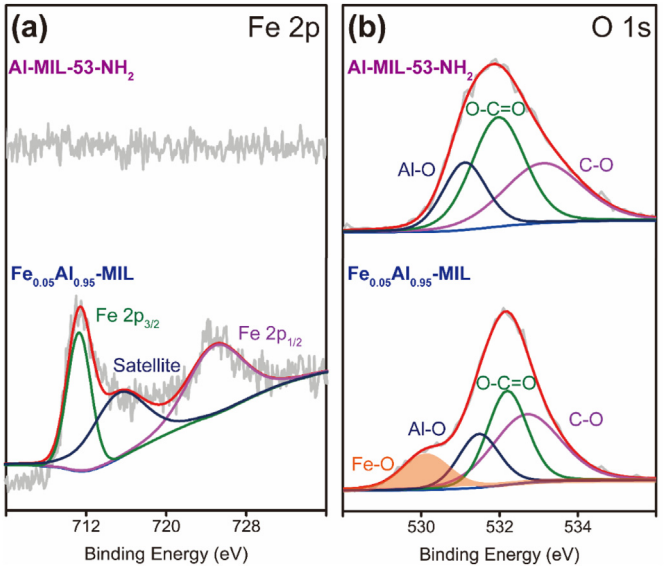

Fig. 3. Fe 2p (a) and O 1s (b) XPS spectra of Al-MIL-53-NH_2 and $Fe_{0.05}Al_{0.95}$-MIL.

Not surprisingly, this increased light absorbance in the visible region with increasing Fe concentration in the Fe_xAl_{1-x}-MIL, is also reflected by color variation changing from light yellow to dark brown. (Fig. 1a-e)

The variation of fluorescence due to the presence of Fe in the bimetallic MOF was investigated by a PL spectrometer. As shown in Fig. 4, the parent MOF Al-MIL-53-NH_2 demonstrated a characteristic blue emission with a maximum peak at 449 nm under the excitation at 330 nm. Detailed excitation and emission spectra are shown in Fig. S2. For the parent MOF Al-MIL-53-NH_2, the luminescence in the framework is centered on the linker BDC-NH_2 since both BDC-NH_2 and Al-MIL-53-NH_2 have similar emission spectra under UV light irradiation (Fig. S3). Within the bimetallic MOF $Fe_{0.05}Al_{0.95}$-MIL, these fluorescence emitting –NH_2 groups were confirmed intact by FT-IR characterization (Fig. S4). However, the fluorescence intensities of Fe_xAl_{1-x}-MIL were reduced significantly, as shown in Fig. 4b. As a transition metal, Al ions within the MOF would induce ligand to metal charge transfer, which is not favorable for the fluorescence generation. Yet, Al-MIL-53-NH_2 with a quantum yield of 14.7% is still observed as compared to $Fe_{0.05}Al_{0.95}$-MIL (QY undetectable). This quenching effect brought upon by the Fe incorporation can be explained as follows. For the light absorption (**I**) process, both Al-MIL-53-NH_2 and $Fe_{0.05}Al_{0.95}$-MIL have nearly the same absorbance values as that of BDC-NH_2 under irradiation, as shown in Fig. 4a, which demonstrates that the absorption process in the MOF occurs on the linker. In addition, the band gaps (E_g) for Al-MIL-53-NH_2 and $Fe_{0.05}Al_{0.95}$-MIL were determined to be 2.77 eV and 2.67 eV (Fig. 5), respectively, further indicating that the partial replacement of Al ions with Fe in MOF has negligible effects on the absorption process. As shown in Fig. 5c, in the emission process (**II**), the spin-allowed transition between the excited singlet state ($\mathbf{S_1}$) to the ground singlet state ($\mathbf{S_0}$) is responsible for the fluorescence emission. Since Fe ions contain unpaired electrons within the matrix of the Al-MIL-53-NH_2, the electrons from the photon-excited organic linker BDC-NH_2 will be transferred into the partially filled d-orbitals of Fe ions. With such strong LMCT competence with linker-based (BDC-NH_2) emission, the fluorescence of as-synthesized Fe_xAl_{1-x}-MIL bimetallic MOF would decrease and even be quenched. Given that increasing incorporated Fe concentration (x = 0.1 and 0.2) does not contribute to further fluorescence quenching (Fig. 4 and Fig. S5), we selected $Fe_{0.05}Al_{0.95}$-MIL as a representative probe for the following H_2S sensing characterization.

The performance of $Fe_{0.05}Al_{0.95}$-MIL towards H_2S detection in an aqueous system was investigated by the addition of different volumes of NaHS solution (1.0 mM) in a 3.0 ml $Fe_{0.05}Al_{0.95}$-MIL suspension. The

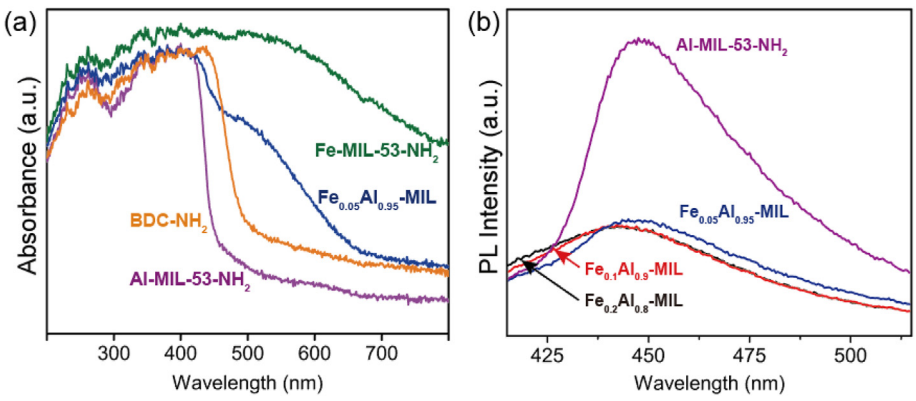

Fig. 4. (a) UV–vis spectra of BDC-NH_2, Al-MIL-53-NH_2, $Fe_{0.05}Al_{0.95}$-MIL, and Fe-MIL-53-NH_2; (b) PL spectra of Al-MIL-53-NH_2 and Fe_xAl_{1-x}-MIL. Excitation wavelength: 330 nm.

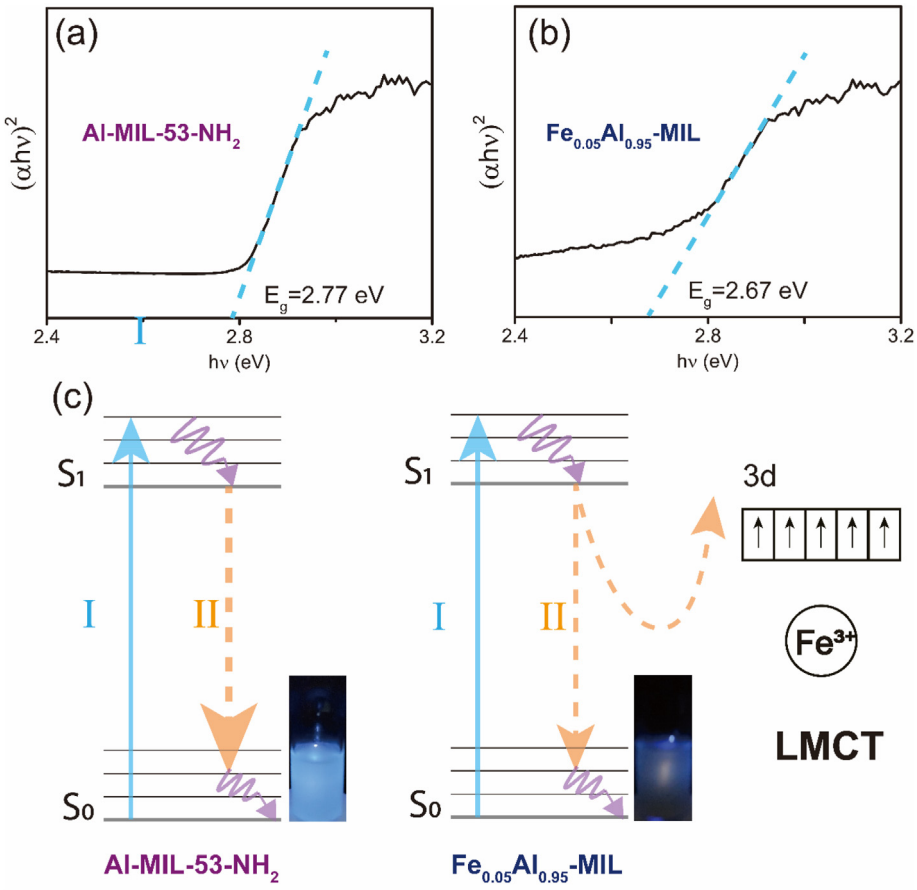

Fig. 5. Tauc plots of bulk Al-MIL-53-NH_2 (a) and $Fe_{0.05}Al_{0.95}$-MIL (b); (c) schematic illustration of energy transfer within the $Fe_{0.05}Al_{0.95}$-MIL. Inset digital images are Al-MIL-53-NH_2 and $Fe_{0.05}Al_{0.95}$-MIL suspensions under UV light (λ = 330 nm).

fluorescence intensity of $Fe_{0.05}Al_{0.95}$-MIL suspension was immediately enhanced after the addition of 20 μL NaHS (1.0 mM); the intensity stabilized within 90 s (Fig. 6a), which is faster than most previously reported H_2S probes [24,26,49]. Additionally, the effect of pH on the $Fe_{0.05}Al_{0.95}$-MIL towards H_2S was studied and the fluorescence intensity remained unchanged when the pH ranged from 3 to 9 (Fig. S6). As depicted in Fig. 6b,c, a very strong linear relationship ($R^2 = 0.9988$) was obtained between the fluorescence intensity of $Fe_{0.05}Al_{0.95}$-MIL and H_2S concentrations (0–38.46 μM). The limit of detection (LOD = $3\sigma/S$) was also determined to be 4.69 μM (Table S2). The above results indicate that the $Fe_{0.05}Al_{0.95}$-MIL can be used for the quantitative H_2S detection in an aqueous system.

The selective sensing of $Fe_{0.05}Al_{0.95}$-MIL on H_2S in water has been validated as well by observation of parallel relations using a variety of common interfering substances. As shown in Fig. 6d, the H_2S analyte showed a significant "turn-on" response, while no additional effects were observed with all selected interferents. Since the $Fe_{0.05}Al_{0.95}$-MIL is already in the "turn-off" mode, typical strong fluorescence quenchers such as transition metal ions ($CuCl_2$, $FeCl_3$, $AlCl_3$, $Co(NO_3)_2$) and oxidative anions (NaF, $K_2Cr_2O_7$) exhibited negligible effects on the fluorescence intensity of the $Fe_{0.05}Al_{0.95}$-MIL sample, as shown in Fig. 6d. It should be noted that no obvious fluorescence changes were observed

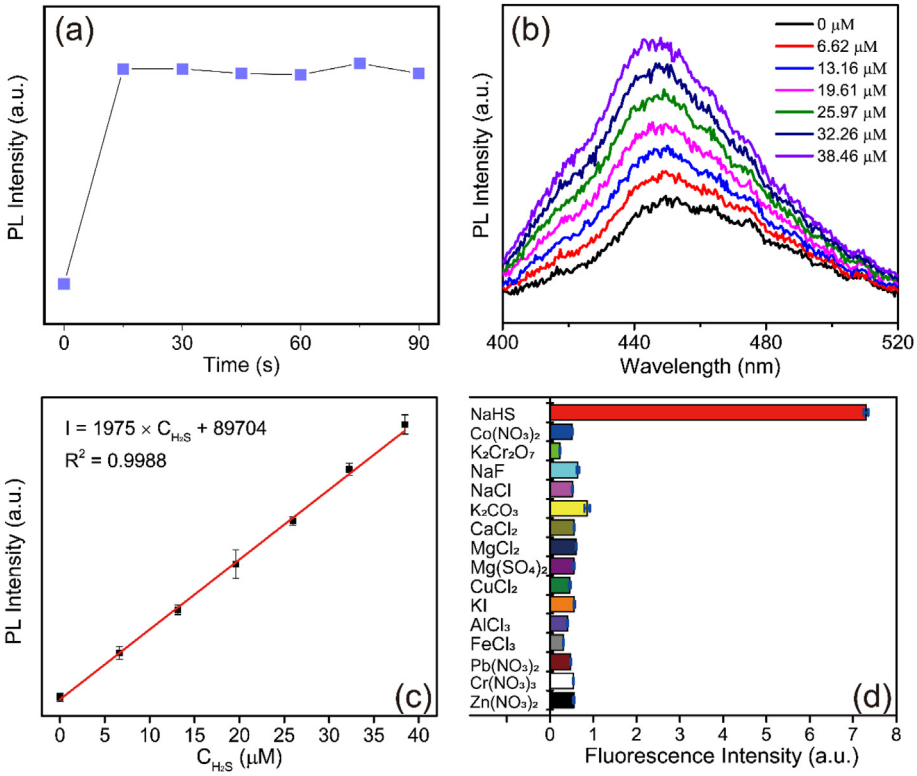

Fig. 6. (a) Fluorescence intensity of $Fe_{0.05}Al_{0.95}$-MIL towards addition of 20 μL NaHS (1.0 mM) after 0–90 s; (b) fluorescence spectra of $Fe_{0.05}Al_{0.95}$-MIL with the increasing concentrations of NaHS (0–38.46 μM) (c) Linear relationship (0–38.46 μM) of the emission intensity of $Fe_{0.05}Al_{0.95}$-MIL enhanced by H_2S; (d) Fluorescence intensity of $Fe_{0.05}Al_{0.95}$-MIL at 449 nm toward various analytes (1 mM).

for some more electrically neutral interferents (NaCl, $CaCl_2$, $MgCl_2$) and reducing interferents (KI) since the Fe^{3+} within the $Fe_{0.05}Al_{0.95}$-MIL is an oxidative agent. All the results discussed above indicate that the as-synthesized bimetallic MOF $Fe_{0.05}Al_{0.95}$-MIL can be used to serve as an excellent sensor for quantitative H_2S detection in complex aqueous systems.

3.3. *"Turn-on" effect exploration*

The "turn-on" effect on $Fe_{0.05}Al_{0.95}$-MIL towards H_2S treatment in an aqueous system was investigated by the analysis of both particles retained in the suspension and supernatant extracts. Detailed experimental information was described in our previous report [50]. The crystallinity of the remaining H_2S-treated $Fe_{0.05}Al_{0.95}$-MIL particles was initially determined by PXRD. As shown in Fig. 7a, the structure of H_2S treated $Fe_{0.05}Al_{0.95}$-MIL was almost completely maintained except for several extra minor peaks and peak ratio variations, which are probably caused by local defects due to the interaction between H_2S and bimetallic MOF. An almost identical FT-IR spectrum of H_2S treated $Fe_{0.05}Al_{0.95}$-MIL was also obtained, indicating that the surface chemistry of the MOF did not alter during the detection (Fig. S7). To identify the reaction site of H_2S during the sensing process, high resolution S 2p scanning by an XPS spectrometer was conducted. As shown in Fig. 7b, no S information was captured for H_2S treated $Fe_{0.05}Al_{0.95}$-MIL particles, while two S related peaks located at 162.2 eV and 167.7 eV were observed from the supernatant extracts; these peaks are likely attributed to Fe–S–O and precipitated sulfide (S), respectively [51]. Additionally, for H_2S treated $Fe_{0.05}Al_{0.95}$-MIL particles, Fe can be hardly observed in the XPS spectrum (Fig. S8) compared to the pristine $Fe_{0.05}Al_{0.95}$-MIL (Fig. 3a), which demonstrated that Fe has been "pulled out" from the framework by H_2S. Moreover, $-NH_2$ groups observed in the FT-IR spectrum (Fig. S9) of supernatant extracts further confirmed that the BDC-NH_2 linker was released during the partial decomposition of bimetallic MOF during H_2S detection. Considering the loss of Fe in H_2S treated $Fe_{0.05}Al_{0.95}$-MIL and the existence of the released BDC-NH_2 linker in the supernatant, the possible reaction process and mechanism could be proposed as follows. During the H_2S sensing process, Fe^{3+} in $Fe_{0.05}Al_{0.95}$-MIL is seized by H_2S rapidly due to the ultrahigh affinity between S^{2-} and Fe^{3+} (ultra-small solubility product constant of Fe_2S_3, 1.4×10^{-88}). The rapid interaction between S^{2-} and Fe^{3+} could also be reflected by the prompt fluorescence deduction within the first 15 s after the addition of NaHS (Fig. 6a). However, the direct reaction product Fe_2S_3 is not stable and could convert to FeS and S immediately; FeS would further be oxidized to Fe^{3+} ($Fe_2(SO_4)_3$) in the presence of air (Fig. 7b). Since Fe nodes were lost through the breakage of the Fe–O bond in the $Fe_{0.05}Al_{0.95}$-MIL framework, the linker was released into the solution (Fig. 7c). Furthermore, PL spectra of both supernatant and resuspended particles were measured again under the same light irradiation. It was found that the supernatant containing the released BDC-NH_2 linkers had the highest fluorescence intensity, while the H_2S treated particles showed negligible contribution to fluorescence enhancement. This is caused by the fact that undissolved H_2S treated $Fe_{0.05}Al_{0.95}$-MIL could absorb and scatter the incident excitation light, thus decrease the fluorescence intensity. Therefore, it can be concluded that the released BDC-NH_2 ligands were real fluorophores that contributed to the fluorescence enhancement.

4. Conclusion

With the assistance of a simple "one-pot" hydrothermal method, a series of bimetallic MOFs, Al_xFe_{1-x}-MIL (x = 0.05, 0.1, and 0.2) have been synthesized for H_2S detection in an aqueous system. Detailed investigations were conducted on bimetallic MOFs including their crystalline structures, optical properties, and H_2S performance. The results showed that only a small amount of secondary Fe^{3+} ions could result in a complete fluorescence quenching in the bimetallic MOF, which could be attributable to the strong LMCT between Fe^{3+} and BDC-NH_2. The

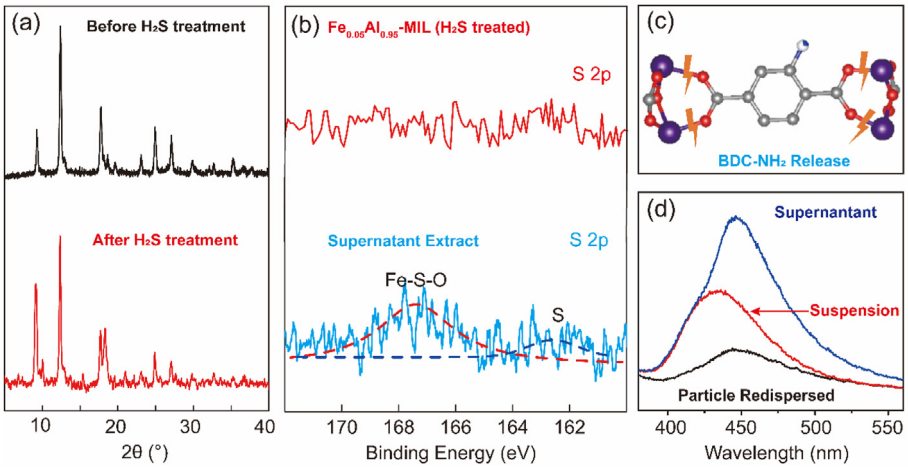

Fig. 7. (a) PXRD patterns of $Fe_{0.05}Al_{0.95}$-MIL before and after H_2S treatment; (b) S 2p spectra of retained H_2S-treated $Fe_{0.05}Al_{0.95}$-MIL particles and supernatant extract; (c) Scheme of BDC-NH_2 released during H_2S treatment; and (d) PL spectra of supernatant, suspension, and particle re-dispersed in water.

response of $Fe_{0.05}Al_{0.95}$-MIL towards H_2S was also tested in an aqueous system. A fluorescence enhancement was observed and a very strong linear relationship was achieved between fluorescence intensity and H_2S concentrations (0–38.46 μM), indicating that $Fe_{0.05}Al_{0.95}$-MIL could be a good candidate for selective and H_2S quantitative detection. Based on the analysis of the H_2S treated bimetallic MOF particles and supernatant, a possible mechanism was explored. During the H_2S sensing process, the secondary Fe^{3+} ions were "pulled out" by S^{2-} from the framework with a concomitant of partial decomposition of bimetallic MOF. The released BDC-NH_2 ligands from the structure were identified to be the real fluorophores responsible for the fluorescence enhancement. Overall, partial substitution of Al ions in Al-MIL-53-NH_2 with secondary Fe^{3+} ions was proved to be an effective method to design a luminescent MOF probe for H_2S detection. We believe this strategy would expand the usage of bimetallic MOFs for chemical sensing applications.

Declaration of competing interest

The authors declare that they have no known competing financial interests or personal relationships that could have appeared to influence the work reported in this paper.

CRediT authorship contribution statement

Zan Zhu: Methodology, Investigation, Data curation, Validation, Conceptualization. **Varun Natarajan:** Data curation, Investigation. **Wei-Ning Wang:** Supervision, Funding acquisition.

Acknowledgments

We are grateful for the financial support from the National Science Foundation (CMMI-1727553).

Appendix A. Supplementary data

Supplementary data to this article can be found online at https://doi.org/10.1016/j.jssc.2020.121434.

References

[1] M.D. Hartle, M.D. Pluth, A practical guide to working with H2S at the interface of chemistry and biology, Chem. Soc. Rev. 45 (22) (2016) 6108–6117.
[2] C.R. Powell, K.M. Dillon, J.B. Matson, A review of hydrogen sulfide (H2S) donors: chemistry and potential therapeutic applications, Biochem. Pharmacol. 149 (2018) 110–123.
[3] Y. Liu, Z. Wei, J. Zhou, Z. Ma, Simultaneous multi-signal quantification for highly precise serodiagnosis utilizing a rationally constructed platform, Nat. Commun. 10 (1) (2019) 5361.
[4] B. Shi, X. Gu, Q. Fei, C. Zhao, Photoacoustic probes for real-time tracking of endogenous H2S in living mice, Chem. Sci. 8 (3) (2017) 2150–2155.
[5] W. Zhao, J. Zhang, Y. Lu, R. Wang, The vasorelaxant effect of H_2S as a novel endogenous gaseous K_{ATP} channel opener, EMBO J. 20 (21) (2001) 6008.
[6] W. Yang, G. Yang, X. Jia, L. Wu, R. Wang, Activation of KATP channels by H2S in rat insulin-secreting cells and the underlying mechanisms, J. Physiol. 569 (Pt 2) (2005) 519–531.
[7] K. Eto, T. Asada, K. Arima, T. Makifuchi, H. Kimura, Brain hydrogen sulfide is severely decreased in Alzheimer's disease, Biochem. Biophys. Res. Commun. 293 (5) (2002) 1485–1488.
[8] A. T, H. D, Y. M, G. D, Relationship between halitosis and periodontal disease – associated oral bacteria in tongue coatings, Int. J. Dent. Hyg. 12 (2) (2014) 145–151.
[9] N. Kumar, V. Bhalla, M. Kumar, Recent developments of fluorescent probes for the detection of gasotransmitters (NO, CO and H2S), Coord. Chem. Rev. 257 (15) (2013) 2335–2347.
[10] Y. Ma, X. Li, A. Li, P. Yang, C. Zhang, B. Tang, H2S-Activable MOF nanoparticle photosensitizer for effective photodynamic therapy against cancer with controllable singlet-oxygen release, Angew. Chem. Int. Ed. 56 (44) (2017) 13752–13756.
[11] B. Yan, Photofunctional MOF-based hybrid materials for the chemical sensing of biomarkers, J. Mater. Chem. C 7 (27) (2019) 8155–8175.
[12] X. Duan, R. Lv, Z. Shi, C. Wang, H. Li, J. Ge, Z. Ji, Y. Yang, B. Li, G. Qian, A new metal-organic framework with suitable pore size and ttd-type topology revealing highly selective adsorption and separation of organic dyes, J. Solid State Chem. 277 (2019) 159–162.
[13] H. Shayegan, Y.D. Farahani, V. Safarifard, A pillar-layer metal-organic framework as a turn-on luminescent sensor for highly selective and sensitive detection of Zn(II) ion, J. Solid State Chem. 279 (2019) 120968.
[14] J. Jiang, Y. Lu, J. Liu, Y. Zhou, D. Zhao, C. Li, An acid-base resistant Zn-based metal-organic framework as a luminescent sensor for mercury(II), J. Solid State Chem. 283 (2020) 121153.
[15] X. Zheng, R. Fan, Y. Song, A. Wang, K. Xing, X. Du, P. Wang, Y. Yang, A highly sensitive turn-on ratiometric luminescent probe based on postsynthetic modification of Tb3+@Cu-MOF for H2S detection, J. Mater. Chem. C 5 (38) (2017) 9943–9951.
[16] Y. Yan, H. Yu, Y. Zhang, K. Zhang, H. Zhu, T. Yu, H. Jiang, S. Wang, Molecularly engineered quantum dots for visualization of hydrogen sulfide, ACS Appl. Mater. Interfaces 7 (6) (2015) 3547–3553.
[17] J. Cui, Y.-L. Wong, M. Zeller, A.D. Hunter, Z. Xu, Pd uptake and H2S sensing by an amphoteric metal–organic framework with a soft core and rigid side arms, Angew. Chem. Int. Ed. 53 (52) (2014) 14438–14442.
[18] S. Li, J. Feng, P. Huang, F. Wu, Cu2+-Mediated turn-on fluorescence assay for sulfide ions using glutathione-protected gold nanoclusters: enhanced sensitivity, good reusability, and cell imaging, New J. Chem. 41 (21) (2017) 12930–12936.
[19] Y. Zhang, S. Yuan, G. Day, X. Wang, X. Yang, H.-C. Zhou, Luminescent sensors based on metal-organic frameworks, Coord. Chem. Rev. 354 (2018) 28–45.
[20] W.P. Lustig, S. Mukherjee, N.D. Rudd, A.V. Desai, J. Li, S.K. Ghosh, Metal–organic frameworks: functional luminescent and photonic materials for sensing applications, Chem. Soc. Rev. 46 (11) (2017) 3242–3285.
[21] Y. Cui, J. Zhang, H. He, G. Qian, Photonic functional metal–organic frameworks, Chem. Soc. Rev. 47 (15) (2018) 5740–5785.
[22] J. Zhao, Y.-N. Wang, W.-W. Dong, Y.-P. Wu, D.-S. Li, Q.-C. Zhang, A robust luminescent Tb(III)-MOF with Lewis basic pyridyl sites for the highly sensitive detection of metal ions and small molecules, Inorg. Chem. 55 (7) (2016) 3265–3271.

[23] Z.-S. Qin, W.-W. Dong, J. Zhao, Y.-P. Wu, Q. Zhang, D.-S. Li, A water-stable Tb(iii)-based metal–organic gel (MOG) for detection of antibiotics and explosives, Inorg. Chem. Front. 5 (1) (2018) 120–126.
[24] S. Nandi, S. Banesh, V. Trivedi, S. Biswas, A dinitro-functionalized metal–organic framework featuring visual and fluorogenic sensing of H2S in living cells, human blood plasma and environmental samples, Analyst 143 (6) (2018) 1482–1491.
[25] S. Nandi, H. Reinsch, S. Banesh, N. Stock, V. Trivedi, S. Biswas, Rapid and highly sensitive detection of extracellular and intracellular H2S by an azide-functionalized Al(iii)-based metal-organic framework, Dalton Trans. 46 (38) (2017) 12856–12864.
[26] S.S. Nagarkar, A.V. Desai, S.K. Ghosh, A nitro-functionalized metal–organic framework as a reaction-based fluorescence turn-on probe for rapid and selective H2S detection, Chem. Eur J. 21 (28) (2015) 9994–9997.
[27] X. Zhang, L. Fang, K. Jiang, H. He, Y. Yang, Y. Cui, B. Li, G. Qian, Nanoscale fluorescent metal–organic framework composites as a logic platform for potential diagnosis of asthma, Biosens. Bioelectron. 130 (2019) 65–72.
[28] X. Zhang, Q. Hu, T. Xia, J. Zhang, Y. Yang, Y. Cui, B. Chen, G. Qian, Turn-on and ratiometric luminescent sensing of hydrogen sulfide based on metal–organic frameworks, ACS Appl. Mater. Interfaces 8 (47) (2016) 32259–32265.
[29] H. Depauw, I. Nevjestić, J. De Winne, G. Wang, K. Haustraete, K. Leus, A. Verberckmoes, C. Detavernier, F. Callens, E. De Canck, H. Vrielinck, P. Van Der Voort, Microwave induced “egg yolk” structure in Cr/V-MIL-53, Chem. Commun. 53 (60) (2017) 8478–8481.
[30] F. Nouar, T. Devic, H. Chevreau, N. Guillou, E. Gibson, G. Clet, M. Daturi, A. Vimont, J.M. Grenèche, M.I. Breeze, R.I. Walton, P.L. Llewellyn, C. Serre, Tuning the breathing behaviour of MIL-53 by cation mixing, Chem. Commun. 48 (82) (2012) 10237–10239.
[31] S. Xu, Y. Ni, NH2-MIL-53(Al) nanocrystals: a fluorescent probe for the fast detection of aromatic nitro-compounds and ions in aqueous systems, Analyst 144 (5) (2019) 1687–1695.
[32] D. Zhao, X.-H. Liu, Y. Zhao, P. Wang, Y. Liu, M. Azam, S.I. Al-Resayes, Y. Lu, W.-Y. Sun, Luminescent Cd(ii)–organic frameworks with chelating NH2 sites for selective detection of Fe(iii) and antibiotics, J. Mater. Chem. 5 (30) (2017) 15797–15807.
[33] C.-X. Yang, H.-B. Ren, X.-P. Yan, Fluorescent metal–organic framework MIL-53(Al) for highly selective and sensitive detection of Fe3+ in aqueous solution, Anal. Chem. 85 (15) (2013) 7441–7446.
[34] A.W. Varnes, R.B. Dodson, E.L. Wehry, Interactions of transition-metal ions with photoexcited states of flavines. Fluorescence quenching studies, J. Am. Chem. Soc. 94 (3) (1972) 946–950.
[35] N. Du, J. Song, S. Li, Y.-X. Chi, F.-Y. Bai, Y.-H. Xing, A highly stable 3D luminescent indium–polycarboxylic framework for the turn-off detection of UO22+, Ru3+, and biomolecule thiamines, ACS Appl. Mater. Interfaces 8 (42) (2016) 28718–28726.
[36] D. Zhang, Y. Guan, E.J.M. Hensen, T. Xue, Y. Wang, Tuning the hydrogenation activity of Pd NPs on Al–MIL-53 by linker modification, Catal. Sci. Technol. 4 (3) (2014) 795–802.
[37] T. Devic, P. Horcajada, C. Serre, F. Salles, G. Maurin, B. Moulin, D. Heurtaux, G. Clet, A. Vimont, J.-M. Grenèche, B.L. Ouay, F. Moreau, E. Magnier, Y. Filinchuk, J. Marrot, J.-C. Lavalley, M. Daturi, G. Férey, Functionalization in flexible porous solids: effects on the pore opening and the Host−Guest interactions, J. Am. Chem. Soc. 132 (3) (2010) 1127–1136.
[38] T. Ahnfeldt, D. Gunzelmann, T. Loiseau, D. Hirsemann, J. Senker, G. Férey, N. Stock, Synthesis and modification of a functionalized 3D open-framework structure with MIL-53 topology, Inorg. Chem. 48 (7) (2009) 3057–3064.
[39] D.Y. Osadchii, A.I. Olivos-Suarez, Á. Szécsényi, G. Li, M.A. Nasalevich, I.A. Dugulan, P.S. Crespo, E.J.M. Hensen, S.L. Veber, M.V. Fedin, G. Sankar, E.A. Pidko, J. Gascon, Isolated Fe sites in metal organic frameworks catalyze the direct conversion of methane to methanol, ACS Catal. 8 (6) (2018) 5542–5548.
[40] Y. Han, J. Zhai, L. Zhang, S. Dong, Direct carbonization of cobalt-doped NH2-MIL-53(Fe) for electrocatalysis of oxygen evolution reaction, Nanoscale 8 (2) (2016) 1033–1039.
[41] J.C. Slater, Atomic radii in crystals, J. Chem. Phys. 41 (10) (1964) 3199–3204.
[42] Y.-y. Zhang, Q. Liu, C. Yang, S.-c. Wu, J.-h. Cheng, Magnetic aluminum-based metal organic framework as a novel magnetic adsorbent for the effective removal of minocycline from aqueous solutions, Environ. Pollut. (2019) 113226.
[43] C.M. Moran, J.N. Joshi, R.M. Marti, S.E. Hayes, K.S. Walton, Structured growth of metal–organic framework MIL-53(Al) from solid aluminum carbide precursor, J. Am. Chem. Soc. 140 (29) (2018) 9148–9153.
[44] W. Guo, W. Sun, L.-P. Lv, S. Kong, Y. Wang, Microwave-assisted morphology evolution of Fe-based metal–organic frameworks and their derived Fe2O3 nanostructures for Li-ion storage, ACS Nano 11 (4) (2017) 4198–4205.
[45] L. Shen, S. Liang, W. Wu, R. Liang, L. Wu, Multifunctional NH2-mediated zirconium metal–organic framework as an efficient visible-light-driven photocatalyst for selective oxidation of alcohols and reduction of aqueous Cr(vi), Dalton Trans. 42 (37) (2013) 13649–13657.
[46] S. Bordiga, C. Lamberti, G. Ricchiardi, L. Regli, F. Bonino, A. Damin, K.P. Lillerud, M. Bjorgen, A. Zecchina, Electronic and vibrational properties of a MOF-5 metal–organic framework: ZnO quantum dot behaviour, Chem. Commun. 20 (2004) 2300–2301.
[47] G.-T. Vuong, M.-H. Pham, T.-O. Do, Direct synthesis and mechanism of the formation of mixed metal Fe2Ni-MIL-88B, CrystEngComm 15 (45) (2013) 9694–9703.
[48] G.-T. Vuong, M.-H. Pham, T.-O. Do, Synthesis and engineering porosity of a mixed metal Fe2Ni MIL-88B metal–organic framework, Dalton Trans. 42 (2) (2013) 550–557.
[49] H. Yu, C. Liu, Y. Li, A. Huang, Functionalized metal–organic framework UiO-66-NH-BQB for selective detection of hydrogen sulfide and cysteine, ACS Appl. Mater. Interfaces 11 (45) (2019) 41972–41978.
[50] Z. Zhu, X. He, W.-N. Wang, Unraveling the origin of the “Turn-On” effect of Al-MIL-53-NO2 during H2S detection, CrystEngComm 22 (2) (2020) 195–204.
[51] Y. Zhan, L. Shen, C. Xu, W. Zhao, Y. Cao, L. Jiang, MOF-derived porous Fe2O3 with controllable shapes and improved catalytic activities in H2S selective oxidation, CrystEngComm 20 (25) (2018) 3449–3454.